Accepted Manuscript

Large ensemble flood loss modelling and uncertainty assessment for future climate conditions for a Swiss pre-alpine catchment

Luise Keller, Andreas Paul Zischg, Markus Mosimann, Ole Rössler, Rolf Weingartner, Olivia Martius

PII: S0048-9697(19)33320-0
DOI: https://doi.org/10.1016/j.scitotenv.2019.07.206
Reference: STOTEN 33400

To appear in: *Science of the Total Environment*

Received date: 7 December 2018
Revised date: 5 July 2019
Accepted date: 13 July 2019

Please cite this article as: L. Keller, A.P. Zischg, M. Mosimann, et al., Large ensemble flood loss modelling and uncertainty assessment for future climate conditions for a Swiss pre-alpine catchment, Science of the Total Environment, https://doi.org/10.1016/j.scitotenv.2019.07.206

Large ensemble flood loss modelling and uncertainty assessment for future climate conditions for a Swiss pre-Alpine catchment

Luise Keller[1], Andreas Paul Zischg[2], Markus Mosimann[2], Ole Rössler[1], Rolf Weingartner[2], Olivia Martius[2]

[1] Institute of Geography, and Oeschger Centre for Climate Change Research, University of Bern, Bern, Switzerland

[2] Institute of Geography, and Oeschger Centre for Climate Change Research, and Mobiliar Laboratory for Natural Risks, University of Bern, Bern, Switzerland

* Correspondence to: luise.keller@giub.unibe.ch

Keywords: flood loss; attribution of uncertainty; surrogate model; climate change; vulnerability function

ABSTRACT

Information on possible changes in future flood risk is essential for successful adaptation planning and risk management. However, various sources of uncertainty arise along the model chains used for the assessment of flood risk under climate change. Knowledge on the importance of these different sources of uncertainty can help to design future assessments of flood risk, and to identify areas of focus for further research that aims to reduce existing uncertainties. Here we investigate the role of four sources of epistemic uncertainty affecting the estimation of flood loss for changed climate conditions for a meso-scale, pre-alpine catchment. These are: the choice of a scenario-neutral method, climate projection uncertainty, hydrological model parameter sets, and the choice of the vulnerability function. To efficiently simulate a large number of loss estimates, a surrogate inundation model was used. 46500 loss estimates were selected according to the change in annual mean precipitation and temperature of an ensemble of regional climate models, and considered for the attribution of uncertainty. Large uncertainty was found in the estimated loss for a 100-year flood event with losses ranging from a decrease of loss compared to estimations for present day climate, to more than a 7-fold increase. The choice of the vulnerability function was identified as the most important source of uncertainty explaining almost half of the variance in the estimates. However, uncertainty related to estimating floods for changed climate conditions contributed nearly as much. Hydrological model parametrisation was found to be negligible in the

present setup. For our study area, these results highlight the importance of improving vulnerability function formulation even in a climate change context where additional major sources of uncertainties arise.

1. INTRODUCTION

Information about future changes in flood losses in a changing environmental and societal system is essential for (flood) adaptation planning and risk management. Flood loss assessments typically rely on coupling several specialised models, including global or regional climate models, hydrological models, inundation models and loss models (see Falter et al., 2015 and Felder et al., 2018 as well as references therein). Along these model chains, various sources of uncertainty exist (Apel et al. 2004; Merz & Thieken, 2009). Epistemic (methodological) uncertainty may be present in the estimation of the flood hazard, e.g. through choice of a certain distribution function for extreme value modelling (Apel et al., 2004; Merz & Thieken, 2009) or through the choice and setup of the (hydrological) models used to derive peak flow magnitudes (Felder et al. 2017; Steinschneider et al., 2015). Likewise, modelling inundation extent and loss is subject to uncertainty that may stem from e.g. the representation of levee failure (Apel et al. 2009) or the formulation of vulnerability models (Apel et al., 2009; Bubeck et al. 2011; Moel & Aerts, 2011). Additional uncertainty when estimating flood loss for future conditions arises from projecting socio-economic development, future land use and climate change.

Estimates of (future) flood loss need to be contextualised by providing adequate uncertainty information. Such information is valuable for i) the user of flood loss estimates in order to prevent maladaptation, ii) to design future assessments of flood loss (e.g. Moel, Bouwer, & Aerts, 2014), and iii) for the research community to identify priority areas for further research that aims to reduce existing uncertainties. In the context of flood loss assessment for future conditions, uncertainty is often considered in form of different scenarios of e.g. socio-economic development or greenhouse gas emissions (e.g. Wing et al., 2018, Alfieri et al., 2015, Arnell & Gosling, 2017, Hattermann et al., 2014). Analysing the possible consequences of such inherently uncertain scenarios may be very valuable, e.g. to motivate climate change mitigation. However, to make progress in the reduction of epistemic uncertainties that arise due to methodological choices, a focus on such sources of uncertainty is necessary. The aim of this study is to quantify the contribution of various methodological uncertainties to the epistemic uncertainty associated with flood loss estimates for changed climate conditions for a pre-Alpine catchment in Switzerland. We do this following an ensemble modelling (e.g. Moel & Aerts, 2011) or parallel models (Merz & Thieken, 2009) approach. That is, we set up a model chain where selected model chain elements are comprised of ensembles of plausible data or methods, and interpret the variability introduced

by the different ensembles as uncertainty.To obtain projections of future flood hazard, we make use of the scenario-neutral approach that allows assessing the effect of a wide range of climate conditions on discharge (e.g. Keller et al. 2019; Prudhomme et al., 2010; Steinschneider et al., 2015). Coupling of the scenario-neutral approach with loss modelling allows appraising flood loss for a wide range of climate conditions and therefore the identification of "high-loss" climate conditions. This may reveal interesting insights as the relationship between flood magnitude and estimated flood loss is not linear, e.g. due to a non-linear increase in the number of exposed assets with increasing flood magnitude or non-linear inundation depth-flood loss relationships. However, methodological choices when performing scenario-neutral flood hazard assessments can have a considerable effect on projected flood peak magnitudes (Keller et al. 2019). We therefore include this source of uncertainty into our analysis together with the projection uncertainty of mean temperature and precipitation change of an ensemble of climate models. In a next step, the meteorological time series obtained with the scenario-neutral approaches are used as input for a hydrological model. Further uncertainties are introduced at that stage that are related to the choice of a hydrological model structure that determines how physical processes are represented (e.g. Dams, Nossent, Senbeta, Willems, & Batelaan, 2015; Karlsson et al., 2016) and to model parametrisation (e.g. Bastola, Murphy, & Sweeney, 2011; Kay, Davies, Bell, & Jones, 2009; Steinschneider et al., 2015). We investigate the importance of hydrological model parametrisation by including a large ensemble of behavioural parameter sets. Subsequently, the projected flood peak magnitudes are coupled to a recently developed surrogate inundation model (Zischg, Felder et al., 2018b; Zischg, Hofer et al., 2018c) that describes the relationship between flood peak magnitude and inundation patterns for the studied floodplain and therefore allows simulating loss for a large number of peak magnitudes. At this stage, we consider the effect of the choice of a vulnerability function which was shown to lead to considerable variability in flood loss estimates (Apel et al., 2009; Bubeck et al., 2011; Felder et al., 2018; Moel & Aerts, 2011, Zischg et al. 2018a). This methodological setup leads to 46500 estimates of future flood loss that represent four sources of uncertainty. These are: scenario-neutral method choice, climate projection uncertainty, hydrological model parameter sets, and choice of the vulnerability function. The importance of each of these uncertainty sources including interactions between them is finally determined by an analysis of variance (ANOVA).

2. STUDY AREA

The assessment of flood loss was conducted for a 55 km^2 floodplain in the lower reaches of the pre-alpine Emme River in Switzerland (see Figure 1 for location of the study area and catchment). The catchment upstream of the study area extends across 963 km^2 with a mean elevation of 860 m a.s.l. Land use in the catchment is dominated by forest (38%) and arable land (32%); pastures account for 20% of the area, and urban areas for 5% (Corine Land Cover 2012, Version 18.5.1). Mean discharge at gauge Wiler is 19 m^3/s and mean annual maximum flood (AMF) peak magnitude is 315 m^3/s for the period 1981-2010 (hourly data). Floods are mostly caused by short, intense rainfall events of several hours, but also longer rainfall as well as rain-on-snow events lead to flooding (Steiner, 2007). The river channel of the Emme is strongly modified by human influence and first simple stability measures date back to the 18th century (TBA OIK IV, 2005). The construction of levees at the end of the 19th century and subsequent river incision lead to a decrease of flood risk in the study area (Zischg, Hofer et al., 2018c). However, settlement growth since the 1960s led to a renewed increase in flood risk (Zischg, Hofer et al., 2018c).

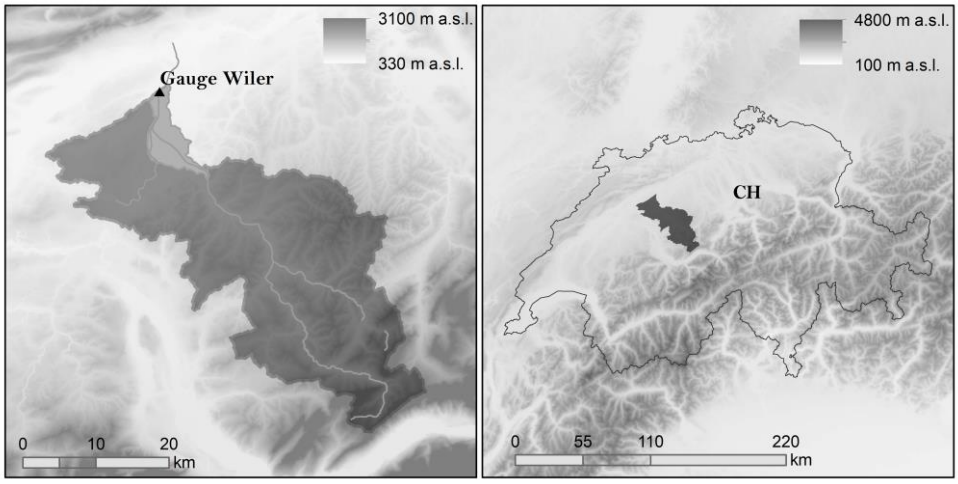

Figure 1 Left: The Emme river catchment with the study area highlighted in light grey. Right: Location of the catchment in Switzerland.

3. METHODS

Our study considers four sources of epistemic uncertainty that affect the estimation of flood loss for changed climate conditions. These are the choice of a scenario-neutral method, climate projection uncertainty, uncertainty related to the parametrisation of the hydrological model, and the choice of the vulnerability function used for the estimation of flood loss. All possible combinations of the four uncertainty sources are used to estimate flood loss following an ensemble modelling approach. The resulting variability of flood loss estimates indicates the overall uncertainty that is captured by our methodological setup. The importance of each of uncertainty source including interactions between them is then determined by an analysis of variance (ANOVA). Figure 2 shows an overview of this modelling chain.

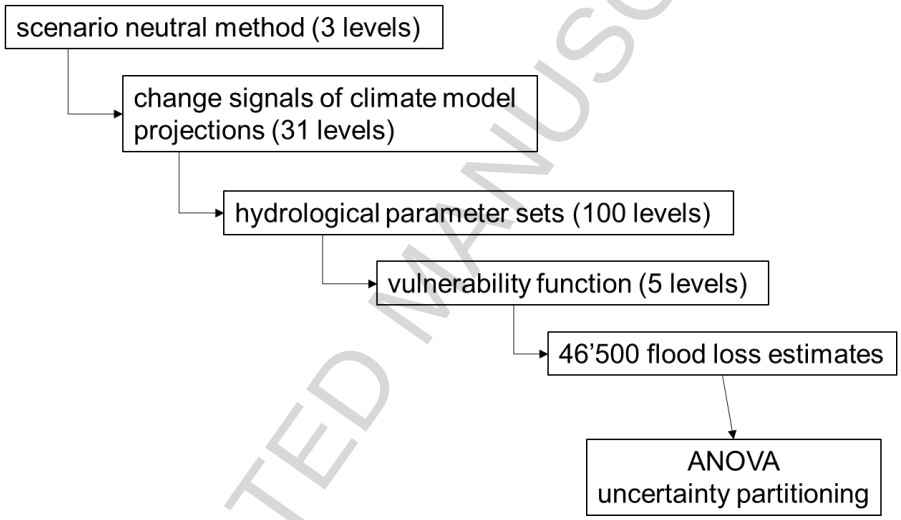

Figure 2: The modelling chain used for analysing the uncertainty associated with the estimation of future flood loss.

In the following, we describe the methods used for generating scenario-neutral projections of temperature and precipitation (section 3.1). Then the calibration of the hydrological model as well as the flood frequency analyses is detailed (section 3.2). In section 3.3 we describe the surrogate inundation as well as the flood loss model. Finally, the method for partitioning the overall uncertainty in the estimation of future flood losses is described (section 3.4).

3.1 SCENARIO-NEUTRAL PROJECTIONS OF TEMPERATURE AND PRECIPITATION

3.1.1. SETUP OF SCENARIO NEUTRAL METHODS

We employed the scenario-neutral approach to obtain projections of future discharge. The scenario-neutral approach is an alternative pathway for climate change impact assessment and can be used to evaluate the sensitivity of a catchment to a wide range of climate conditions. The term "scenario-neutral" refers to the shift from using climate model-based scenarios for impact assessment to an impact assessment based on sensitivity analysis (Prudhomme et al., 2010). Performing a scenario-neutral impact assessment requires choosing a set of meteorological variables (e.g. temperature, precipitation) that are altered, and a suitable method for generating time series representing altered climate conditions of the selected variables. The hydrological response to these time series is subsequently modelled with a hydrological model. Keller et al. (2019) showed that considerable uncertainties are introduced by the choice of scenario-neutral method and we thus investigate the role of scenario-neutral method choice in shaping flood risk uncertainty. We employed three different scenario-neutral methods for deriving projections of temperature and precipitation that are summarised in Keller et al. (2019). These are: Seasonal scaling (Prudhomme et al., 2010), regional climate model (RCM) scaling (Vormoor et al., 2017), and weather generator (WG) scaling (Steinschneider et al., 2015). The meteorological time series generated with the three methods represent change in mean annual values as well as in several additional attributes of temperature and precipitation change. Additional attributes of climate change are all attributes of precipitation and temperature other than their mean such as their seasonal cycle or daily extremes.

The same range of change in mean precipitation and temperature was considered for the three methods: Increase in annual mean temperature was considered in the range of +1°C to +7°C by increments of 1°C relative to the 1981-2010 average. Annual mean precipitation was altered by -20% to +20% by increments of 10% relative to the same reference period. That is, we consider 7 x 5 = 35 scenarios of mean change in precipitation and temperature. In addition, seasonal scaling incorporates change in the seasonal cycle of temperature and precipitation. RCM scaling incorporates change of precipitation occurrence (e.g. dry/wet spell durations) as well asprecipitation variability by using RCM time series representing a selected future period. WG scaling is used to scale daily precipitation extremes as well as to consider the effect of natural variability on projected peak magnitudes. Information on likely changes in the seasonal cycle and precipitation extremes are taken from projections of an ensemble of climate model data. To this end, we used bias corrected climate model output from an ensemble of 31 GCM-RCM combinations from the EURO-CORDEX initiative (Jacob et al., 2014).

GCMs were forced with greenhouse gas concentration (GHG) trajectories according to RCP8.5, and RCMs run at ~12 km (EUR11) or ~50km (EUR44) grid spacing (see table 4.1 in CH2018, 2018 for an overview of the models used). Climate model projections were downscaled to a 2 km grid and bias-adjusted using quantile mapping(CH2018, 2018). While it is not compulsory to use climate model data when applying a scenario-neutral method (note that the RCM scaling is an exemption to the general case in that it relies on climate model time series), it allows comparing the projections obtained by the different methods to each other.

In the following, we provide a short summary of the scenario generation for each of the three methods. For further details the reader is referred to Keller et al. (2019) and the references therein. Please note that if not stated otherwise we use the term "scenario" to refer to the meteorological time series derived from the scenario-neutral method throughout this study.

3.1.2. SEASONAL SCALING

To generate time series representing changes in the intra-annual cycles of precipitation and temperature, observed time series of the precipitation and temperature are scaled with daily change factors (CF, i.e. additive or multiplicative adjustment of values). Change factors were derived by first determining change in monthly mean precipitation and temperature for each of the 31 climate model projections between the future (2070-2099, in the following "scenario-period") and the reference period (1981-2010) time series. Then, the intra-annual patterns of change extracted from the climate models are represented by fitting a simple cosine function (Equation (1)) to the monthly change values. The resulting patterns are summarized in Table 1 in terms of the cosine function parameters amplitude and phase together with the number of occurrences of the respective pattern of change in the climate model ensemble. Finally, the intra-annual patterns were combined with the 35 scenarios of mean change by scaling the cosine function´s mean accordingly. This resulted in 35 x 31 scenarios of seasonality represented by 1085 cosine functions.

$$y_t = \overline{y} + C_1 \cos\left(\frac{2\pi t}{12} - \Phi_1\right) \quad (1)$$

with y_t – change factor of month t, $\overline{y}$ – mean of monthly change factors, C_1 – amplitude, Φ_1 – phase.

From each cosine function, daily CFs were derived that were used to scale the 30-year observational time series representing today's climate (1981-2010).

Table 1: Cosine function parameters describing the intra-annual cycle of precipitation and temperature change. Parameters were obtained by fitting a simple cosine function to the 30-year average of monthly temperature and precipitation change, respectively, for each of the 31 climate models. Each row describes a seasonal pattern and the number of occurrences of each pattern among the 31 climate models is indicated in the right column. Phase values were set to the centre of the season the parameter fell into (e.g. 15th January for DJF). Amplitudes were rounded to the closest decadic value for precipitation and to the closest integer value for temperature.

Precipitation change		Temperature change		Number of occurrences
Amplitude [%]	Phase	Amplitude [%]	Phase	
10	April	1	October	1
10	January	1	October	1
10	January	1	April	1
10	January	0	-	1
20	January	0	-	6
20	April	1	October	3
20	January	1	October	2
20	April	0	-	2
30	January	0	-	2
30	January	1	October	3
30	April	1	October	3
30	January	1	July	1
40	January	1	October	1
50	January	2	October	1
50	January	1	October	2
60	January	1	October	1

3.1.3. WG SCALING

For the third method, quantile mapping was used to change the mean and extremes of precipitation time series that were simulated with a weather generator. We used the stochastic weather generator LARS-WG (Semenov & Barrow, 1997; Semenov, Brooks, Barrow, & Richardson, 1998) to generate 100 time series of 30-year daily minimum and maximum temperature, and daily precipitation amounts. The weather generator was calibrated for reference period conditions using observation-derived areal mean precipitation, minimum, and maximum temperature (Frei et al., 2006; Frei, 2014). Resulting daily minimum and maximum temperature time series were averaged to obtain daily mean temperature that is needed for the hydrological model.

To change daily precipitation extremes while controlling for the mean, the coefficient of variation is scaled (CV). Scenarios of CV change were derived by determining change of annual precipitation CV from the climate model projections. See Table 2 for the resulting CFs. These were used to scale the precipitation time series as summarised in the following. First, gamma functions were fitted to the monthly non-zero precipitation data for

each WG precipitation time series. Then, the mean and variance of each distribution were scaled accounting for the different CFs of CV and mean change. Finally, quantile mapping was used to transform the weather generator time series according to the derived distribution. Temperature time series were scaled to different annual mean values by additive scaling. In total, we obtained 31x 35 x 100 = 108500 scenarios for the WG scaling

Table 2: Change factors of annual precipitation CV derived by comparing scenario and reference period time series of the 31climate models together with the number of occurrences of each change factor among the models. Change factors were rounded to closest integer multiple of 5%.

CF of annual precipitation CV [-]	0.95	1	1.05	1.1	1.15
Number of occurrences	1	6	11	11	2

3.2 HYDROLOGICAL MODELLING

3.2.1. CALIBRATION OF THE HYDROLOGICAL MODEL

Discharge was simulated on a daily time step using the lumped, conceptual GR6J model (Pushpalatha et al., 2011) that has six free parameters. In addition, we used a routine for snow accumulation and melt (CemaNeige; Valéry et al., 2014) that introduces two additional free parameters. CemaNeige GR6J was calibrated against observations of daily mean discharge for the period 1981-2014 (excluding a two year spin-up period) and using interpolated daily precipitation amounts and daily mean temperature data (see Frei et al., 2006 for details on precipitation interpolation scheme and Frei, 2014 for details on temperature interpolation). To account for uncertainty in the parametrisation of the model, 100 behavioural parameter sets were identified using a local steepest gradient algorithm implemented in GR6J. This was done in two steps: In a first step, we used the Nash-Sutcliffe-Efficiency (NSE) of ordered discharge values as objection function, i.e. a calibration based on ranked discharge magnitudes rather than on the discharge time series (e.g. Paquet et al., 2013). Minimizing the NSE of ordered discharge values led to a better correspondence between the high values of simulated and observed discharge compared to the use of non-ordered discharge data as illustrated in Figure 3.

The focus was set on high discharge values as only annual maximum discharge values were used for the subsequent analysis. In a second step, NSE was minimized with regard to the (non-ordered) discharge time series to ensure plausible model results in the time domain also. For the first step, local optimization was done for 6561

initial parameter sets (i.e. a modification of the calibration algorithm implemented in the GR6J, which only uses the best performing parameter set out of the 6561 initial sets for local optimization). The set of initial parameter sets represents all combinations of the 16.5^{th}, 50^{th} and 83.5^{th} quantiles of empirical derived parameter distributions for each parameter and was taken from GR6J code (version 1.0.9.64). For all 6561 initial parameter sets, local optima were found that led to a NSE of sorted discharge values above or equal to 0.99. In the second step, we selected the best 100 parameter sets with regard to the NSE of non-ordered discharge data. The resulting parameter sets lead to NSE values of 0.72 for the calibration period and in the range of 0.71-0.72 for the validation period (1963-2014).

3.2.2. FLOOD FREQUENCY ESTIMATION

Quantile mapping of AMF peak magnitudes

Runoff simulated using climate model or weather generator (WG) time series as input can contain considerable bias compared to observation-forced simulations with the same hydrological model setup (Keller et al., 2019). For our study, we found that mean annual maximum flood (AMF) peak magnitudes were overestimated by about 13% on average using the 31 climate model reference period time series and underestimated about 15% on average using the 100 weather generator derived time series. To avoid propagating theses biases through the subsequent analysis steps, we performed a quantile mapping of observed AMF peak magnitudes to represent projected changes of AMF instead of directly using projected AMF. This is done under the assumption of a stationary bias. We first derived empirical cumulative distribution functions (cdf) of simulated AMF for the reference period 1981-2010 (for the observational, climate model and WG time series, respectively) and for the climate change scenarios generated by the three scenario-neutral methods. For each scenario-neutral method, scenario of climate change, and hydrological model parameter set, we then determined the change of AMF by comparing the scenario cdf to the respective reference period cdf. Change between the cdfs was calculated for 10% intervals of non-exceedance probability to increase robustness of the results (i.e. change for each 10% interval is determined by the average change of three events when using a 30-year series of AMF). The change factors obtained were then used to scale the empirical cdf of observed AMF peak magnitudes (period 1981-2010).

Peak flow estimation and extreme value modelling

Hydrological modelling was carried out using a daily time step because both climate model projections and WG data were available at daily resolution only. Hydrodynamic modelling on the contrary was based on flood event hydrographs that represent instantaneous peak flows (IPF). Thus, to link the two models, IPF had to be estimated based on daily mean flows. For this, a scaling factor was derived by fitting a linear model between observed hourly and daily mean runoff at the gauge Wiler for a sample of flood events. The sample of flood events was derived from observed discharge of the period 1974-2014 by selecting all days with daily mean flow above 100 m^3/s. This threshold corresponds roughly to the 10^{th} quantile of AMF events in the period. With this procedure, 87 events were identified and used for the linear regression. All events were separated by at least 12 days so that we can assume independence of the events.

After the estimation of IPF, extreme value modelling was carried out for each simulation. We fitted generalized extreme value distributions to the IPF estimates using a modified version of the maximum-likelihood method (Martins & Stedinger, 2000). Only the 100-year event was considered for subsequent analysis. To estimate the loss corresponding to these events, we aggregated the results from the scenario-neutral methods by taking the median of the 100-year return values across the additional attribute scenarios. That is, for each scenario-neutral method and parameter set we obtained 54 estimates of the 100-year event corresponding to the 54 scenarios of change in annual mean temperature and precipitation.

3.3 SURROGATE INUNDATION MODEL AND VULNERABILITY FUNCTIONS

Simulating flood wave propagation with two-dimensional hydrodynamic models at a high spatial resolution may not be feasible for the simulation of large ensembles of scenarios due to the large computational demands that can arise (Moel et al., 2012; Zischg et al., 2018b). A way to reduce the computational burden of resource intensive modelling tasks is the use of surrogate models. Surrogate models are simplified, computationally cheaper versions of the original model where simplification can be achieved either by approximating the model output by data-driven function-approximation techniques, or by developing less-detailed versions of the original physically based model (Razavi, Tolson, & Burn, 2012b). Surrogate models are used for a variety of applications that involve large numbers of model runs like optimization and sensitivity analysis (see Ratto, Castelletti, & Pagano, 2012 and Razavi, Tolson, & Burn, 2012a for an overview). For the present study, we use a previously developed surrogate inundation model that describes the relationship between flood peak magnitudes and inundation patterns in the study area (Zischg et al., 2018b; Zischg et al., 2018c). The surrogate model synthesises

the outcome of a number of flood inundation simulations with a two-dimensional inundation model of very high spatial resolution (cell size of the digital terrain model 0.5 m) into a simpler and fast-to-run meta-model. It thus enables the estimation of flood loss for large ensembles of simulations. It has been developed in three steps that are summarised shortly here: In a first step, synthetic design hydrographs were derived for flood peak magnitudes between 200 m^3/s and 1400 m^3/s with an interval of 50 m^3/s (range of peak magnitudes extended compared to Zischg et al., 2018c). In a second step, inundation patterns were simulated for each of the synthetic design hydrograph using the two-dimensional hydrodynamic model. In a third step, each inundation simulation was superimposed with building data (see Röthlisberger et al., 2017, 2018 for details on the building data) and maximum flow depths resulting from the respective inundation simulation were attributed to each individual house as suggested by Bermudez & Zischg (2018). The resulting surrogate inundation model allows the rapid determination of the inundation patterns for a given flood peak magnitude.

To estimate object-specific losses due to structural damage to the buildings for the projected flood peak magnitudes, the flow depths at the building were combined with a set of vulnerability functions. A selection of vulnerability functions was used as there is no vulnerability function available that is specifically developed for the study area. In addition, lack of validation data hinders the identification of the most suitable function for the studied floodplain. The chosen vulnerability functions estimate the degree of loss (0 for no loss, 1 for total loss) on the basis of the flow depth at the building. Five vulnerability functions that have been used in several studies that estimate flood loss in Swiss catchments (Felder et al., 2018; Zischg et al., 2018a,b,c) were considered for the present study (Figure 4), namely the functions of Totschnig et al. (2011), Papathoma-Köhle et al. (2015), Hydrotec (2011), Jonkman et al. (2008), and Dutta et al. (2003). For each building and vulnerability function, the loss corresponding to a given inundation level was derived by multiplying the degree of loss with the specific reconstruction value of the building (see Röthlisberger et al., 2018 for details on the building values). Finally, all losses in the study area were summed up for a given inundation simulation.

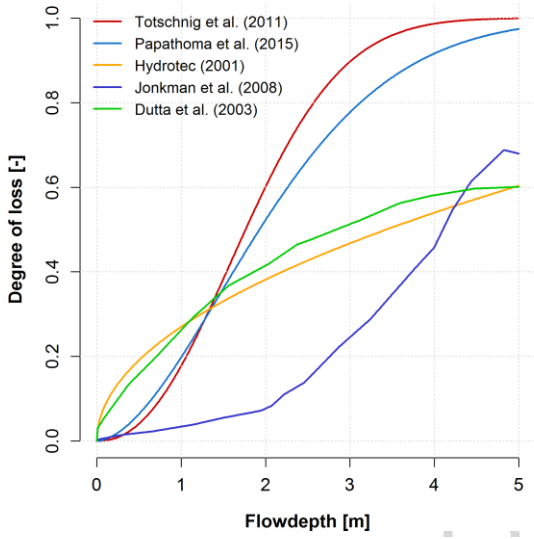

Figure 3: Vulnerability functions used in this study.

3.4 UNCERTAINTY PARTIONING

To assess the contribution of each of the four uncertainty sources to the overall uncertainty, we performed an ANOVA. For this purpose we reduced the scenarios of annual mean precipitation and temperature change to those corresponding to the 31 climate model projections. Thus, 46500 estimates of flood loss representing four sources of uncertainty (called factors in the ANOVA setting) were used for the ANOVA: Scenario-neutral methods (3 levels)

- Change signals of the climate model projections in terms of annual mean temperature and precipitation change (31 levels)
- Vulnerability functions (5 levels)
- Hydrological model parameter sets (100 levels)

The variance explained by each factor is determined by calculating the ratio of sum of squares of each factor to the total sum of squares (Bosshard et al., 2013). To reduce the bias in the sum of squares calculation introduced by the different number of levels of the four factors, we performed ANOVAs on subsamples of the data similar to Bosshard et al. (2013). To do so, we constructed 10.000 subsamples of loss estimates by drawing three change signals of mean precipitation and temperature, three vulnerability functions, and three model parameter sets. For each subsample, we derived the fraction of explained variance for each factor, their second-order interactions

(i.e. interaction between two factors) and the residuals. The overall variance contribution of each factor was finally derived by taking the mean of the subsample estimates. Results

3.5 PROJECTED FLOOD PEAK MAGNITUDES

Figure 5 shows the median flood peak magnitudes resulting from forcing the hydrological model with the scenario-neutral projections of temperature and precipitation change. Depicted are the flood peak magnitudes corresponding to a return period of 100-years for each of the three scenario-neutral approaches. RCM scaling leads to the highest median peak magnitudes for a given scenario of mean temperature and precipitation change whereas projections from seasonal scaling and WG scaling are more alike on average. Maximum difference in projected peak magnitudes for a given scenario of mean change amounts to 175 m^3/s. An increase in mean temperature tends to reduce projected peak magnitudes, though the effect is small generally and especially for the seasonal scaling. In the context of the scenario-neutral approach, an increase in temperature is not associated with an increase in precipitation extremes per se. Change in precipitation extremes and other additional attributes of precipitation and temperature are considered by the respective scenarios (see section 3.1, results not shown here).

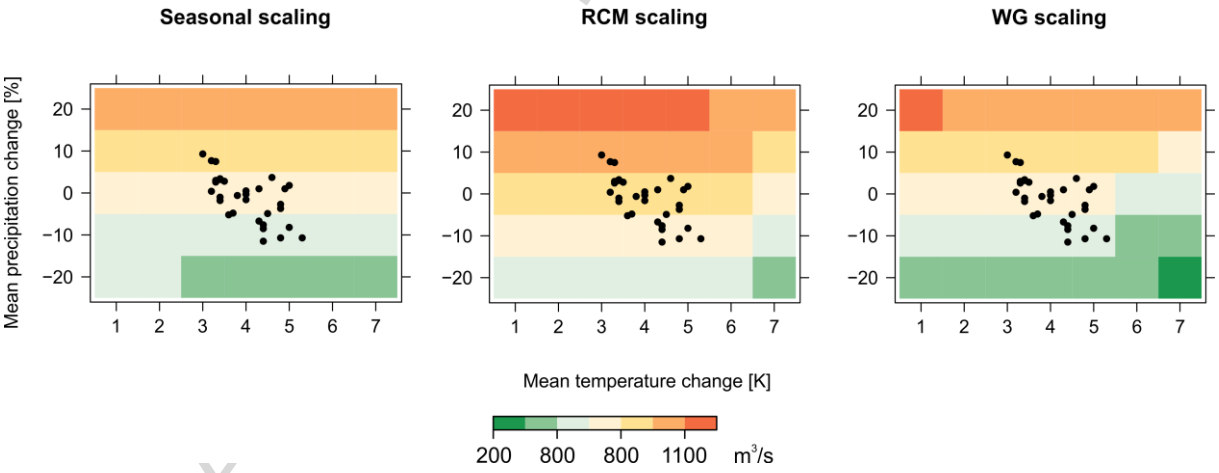

Figure 5: Response surfaces of the median 100-year flood as a function of annual mean temperature and precipitation change. Each panel shows the results from one scenario-neutral method. Return values of the 100-year events were averaged across the additional attributes scenarios of temperature and precipitation change (see section 3.2.2) and hydrological parameter sets. Black dots indicate annual mean temperature and precipitation change according to the 31 climate models.

3.6 SURROGATE INUNDATION MODEL AND FLOOD LOSS ESTIMATION

Figure 6a summarises the output of the surrogate inundation model by showing the number of exposed buildings and mean inundation depths at the exposed buildings in the study area as a function of flood peak magnitude. Average flow depth increases sharply for peak magnitudes up to 300 m^3/s as only one building closely located to the weak point in the levee is affected. There is little variation in the average flow depths for peak magnitudes above 600 m^3/s. This is a consequence of the relatively flat topography of the study area where increasing flood magnitudes rather lead to an increase of flooded area than of flow depth at the buildings. The relationship between peak magnitude and flood loss for the five vulnerability functions considered is shown in Figure 6b. Loss estimated for a given peak magnitude is a function of the value of the buildings affected and of the degree of loss determined by inundation depth and vulnerability function. Below peak magnitudes of 400 m^3/s almost no damage occurs as few buildings are affected (cf. Figure 6a). Increase in loss estimates above this peak discharge is mainly driven by an increase in the number of exposed buildings as the mean inundation depth at the exposed buildings remains approximately constant. Thus, the increasing differences between the loss estimates of the five vulnerability functions for increasing flood magnitudes apparent in Figure 6b are mainly a function of the number of exposed buildings rather than of changes in the degree of loss.

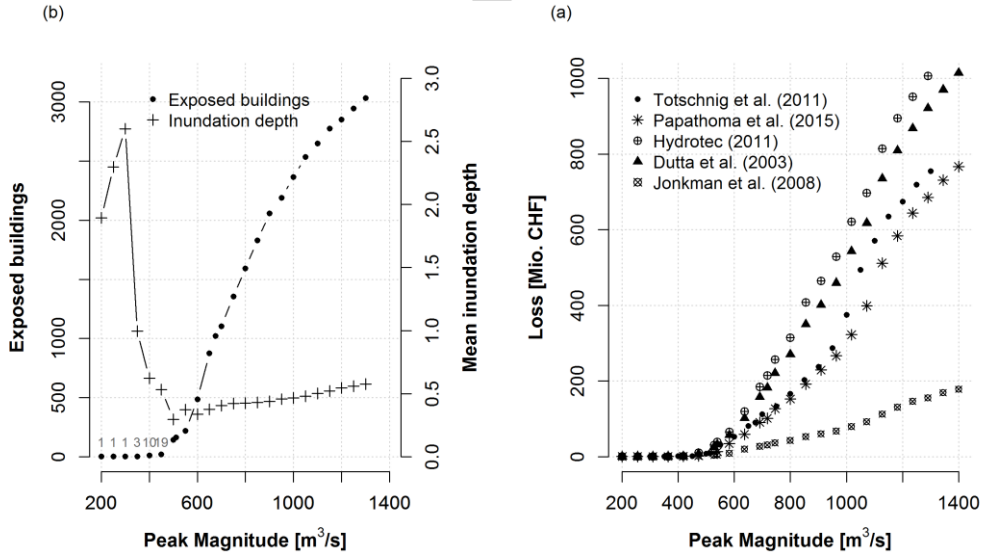

Figure 6: (a) Number of exposed buildings and mean inundation depth at exposed buildings as a function of peak magnitude. Grey numbers indicate number of exposed buildings for the first six values of peak magnitude. (b) Total loss in the study area as a function of peak magnitude for five different vulnerability functions.

3.7 SENSITIVITY OF LOSS ESTIMATES TO CLIMATE CHANGE

Figure 7 shows the average loss estimates for the median 100-year flood event for each of the three scenario-neutral methods as a function of annual mean temperature and precipitation change. The range of loss estimates across the scenarios is similar for RCM and WG scaling while both the range and maximum values are lower for the seasonal scaling. Maximum flood loss (resulting from a precipitation increase of 20% and temperature increase of 1°C) differs by approximately 270 Mio. CHF between the seasonal and the RCM scaling. Differences between the methods decrease with decreasing values of precipitation change. For mean precipitation and temperature change according to the climate models (black dots in Figure 7), loss estimates of seasonal and WG scaling are in the same order of magnitude. Maximum loss for these scenarios is ~240 Mio. CHF for the seasonal and WG scaling, and ~370 Mio. CHF for the RCM scaling (for +3°C and +20%). Some of the scenarios corresponding to the climate model change signals indicate a decrease of loss compared to the reference period (magnitude of reference period loss indicated by grey line in the colour scale of Figure 7).

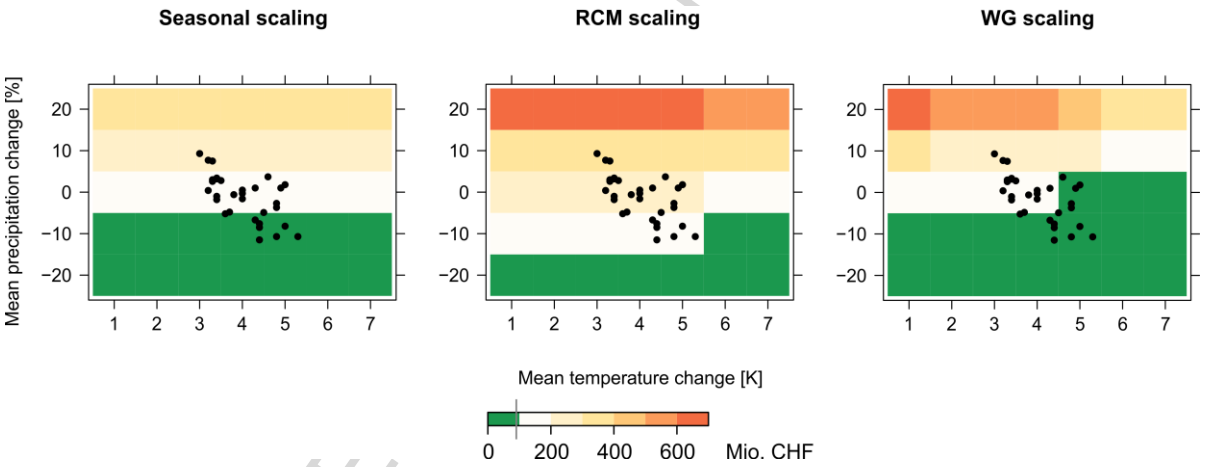

Figure 7: Response surfaces of average flood loss for the median 100-year flood as a function of annual mean temperature and precipitation change. Each panel shows the results from one scenario-neutral method. Return values of the 100-year events were averaged across the additional attributes scenarios of temperature and precipitation change (see section 3.2.2). Loss estimates were averaged across hydrological parameter sets and vulnerability functions. Black dots indicate annual mean temperature and precipitation change according to the 31 climate models.

3.8 INFLUENCE OF VULNERABILITY FUNCTIONS ON FLOOD LOSS PROJECTIONS

Figure 8 illustrates the influence of the choice of the vulnerability function on loss estimates for the median 100-year event. Shown are estimates for all scenario-neutral methods and the scenarios of mean temperature and precipitation change corresponding to the climate model change signals (cf. black dots in Figure 7). The distributions vary greatly with respect to the median and interquartile range. Median estimates differ by 240 Mio

CHF at maximum and by 160 Mio. CHF when only the four highest estimates are considered (i.e. if the function of Jonkman et al., 2008 is excluded). The spread of the distributions indicate the sensitivity of the vulnerability functions to changes in the inundation extent (cf. Figure 6): Loss estimates for the different scenarios lie within ~90 Mio. CHF using the vulnerability function after Jonkman et al. 2008 whereas estimates vary by more than 600 Mio. CHF using the vulnerability function after Hydrotec (2011). Note that difference between the methods depends on the return period of the flood event. For smaller peak magnitudes, differences between the loss estimates of the vulnerability functions decrease (cf. Figure 6).

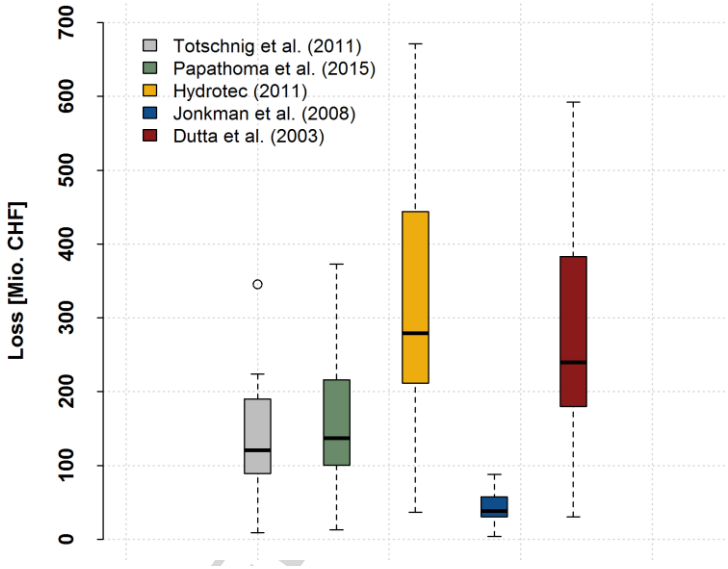

Figure 8: Distribution of flood loss estimates for the five different vulnerability functions for the median 100-year event. Each boxplot shows the distribution of loss estimates across all SN methods and using the scenarios of annual mean temperature and precipitation corresponding to the climate models. Loss estimates are averaged across the different hydrological model parameter sets.

3.9 UNCERTAINTY PARTIONING ALONG THE FLOOD LOSS MODELLING CHAIN

The total uncertainty in the loss estimate for the 100-year flood is ~670 Mio. CHF. This uncertainty was partitioned into contributions of the four factors and their interactions in the following way: Vulnerability functions are the largest source of variation explaining 48% of the total variance. Uncertainty related to the projection of flood loss for changed climate conditions (i.e. due to the change signal of the climate model ensemble and due to the scenario-neutral method) amounts to 42% of total variability. The choice of a hydrological model parameter set has virtually no effect on the loss estimates. All second order interactions together explain 10% of total variability. This uncertainty can largely be attributed to the interactions between

vulnerability functions and scenario-neutral methods, and between vulnerability functions and change signals(each explains ~5% of total variance). In section 4.4 it was shown that scenario-neutral method choice and change signals influence the differences between vulnerability functions (indicated by the different spread of the distributions). Here we quantified this interaction effect for both factors.

Table 3: Proportion of the total variance of the flood loss estimates for the 100-year event explained by the different factors, their interactions, and residuals.

	SN Method	CS RCMs	Vulnerability Function	Model Parameter	Interactions	Residuals
Explained Variance [%]	21	21	48	0	10	0

SN-scenario neutral, CS- change signal, RCM – regional climate model

4. DISCUSSION

Several studies assess the role of hydrological model parametrisation as an uncertainty source in the estimation of flood peak magnitudes for changed climate conditions (e.g. Bastola et al., 2011; Chen, Brissette, Poulin, & Leconte, 2011; Kay et al., 2009). Some studies find that the variability due to different parameter sets is considerable for lower frequency events (return periods of 50 to 100 years) and in some catchments (Bastola et al., 2011; Jung, Chang, & Moradkhani, 2011). Other studies point to a minor role of hydrological model parametrisation in shaping overall uncertainty of flood projections compared to other sources of uncertainty like the choice of the emission scenario, general circulation model, downscaling and hydrological model structure (Chen et al., 2011; Kay et al., 2009). Our results indicate a negligible contribution of hydrological model parameter sets to the overall uncertainty. However, these results may depend on the hydrological model, the method to derive parameter sets and the catchment properties.

Another source of uncertainty considered in the present study was the choice of a scenario-neutral method. Considerable differences emerged in the estimates of 100-year flood peak magnitudes and flood loss between the methods (up to 175 m^3/s and ~270 Mio. CHF of maximum difference between the methods for a given climate change signal). Keller et al. (2019) compared the same three scenario-neutral approaches with regard to projections of annual maximum flood peak magnitudes for another pre-alpine catchment in Switzerland. Although the study of Keller et al. is not directly comparable to the present study due to different input data,

their conclusion that scenario-neutral method choice can introduce considerable uncertainty, is confirmed here. In addition, we extended the study of Keller et al. on the effects of the scenario-neutral approach on climate change impacts to considering flood losses. This allowed the assessment of the role of the scenario-neutral approach in shaping overall uncertainty in the estimation of future flood losses.

An evolving body of literature assesses the role of the choice of the vulnerability function for flood loss estimation uncertaintys. While Merz & Thieken (2009) found that extreme value modelling and inundation modelling contribute more to overall uncertainty in flood damage estimates than vulnerability models over a range of return periods, other studies regard vulnerability functions as one of the most relevant sources of uncertainty in flood loss estimation (Bubeck et al., 2011; Moel & Aerts, 2011). This is especially true for inundation depth-damage functions (Apel et al., 2009). Our study suggests that the choice of the vulnerability function has a greater influence on future flood loss estimatates than all other factors considered. However, if we jointly consider the factors that represent uncertainty due to assessing the impact of climate change (i.e., scenario-neutral method choice and climate model change signals), they explain almost as much variation as the vulnerability functions. While our analysis covers a wide range of existing depth-damage functions many others exist (see Gerl et al., 2016 for a review). The relevant contribution of the vulnerability function to the overall uncertainty in flood loss estimation points out that flood reduction policies aiming at protecting properties from flooding by structural measures at the building level offer a high potential in future flood risk reduction.

An important limitation to the generalisation of our results is their dependence on the study area. The loss estimates are influenced by the characteristics of the floodplain such as its morphology, the distribution of buildings as well as of the building values. For example, the morphology of a river and of its floodplain influences inundation depths and thus the sensitivity of loss estimates to vulnerability function (as the latter predict the degree of loss as non-linear functions of inundation depth). For the Emme floodplains considered here, mean inundation depth remained below 0.6 m even for the highest simulated peak discharges and thus differences in the estimated degree of loss below 20% (see Figure 6). For floodplains in narrow river valleys where inundations depths increase more strongly with increasing peak magnitudes, larger variability in estimated loss would be introduced using our set of vulnerability functions (cf. Figure 4).

Our results are conditional on several assumptions and modelling choices. One of these is the emission scenario we considered. Our ensemble of climate models was forced with the GHG emissions trajectory corresponding to RCP8.5. These trajectories assume the strongest increase in GHG emissions compared to other trajectories. For Switzerland, RCP8.5 generally leads to stronger changes in precipitation extremes compared to RCP4.5 and

RCP2.6 (CH2018, 2018). Thus, it could be speculated that using another RCP would lead to a smaller contribution of climate model change signals and scenario-neutral method choice to overall uncertainty (as the scenario generation for the latter is influenced by the climate model data).

Further assumptions were made which would themselves constitute important topics for additional uncertainty analysis. One of those is the method for deriving peak magnitudes from daily mean flow. As sub-daily regional climate model projections still lack reliability with regard to e.g. the representation of rainfall extremes (Gregersen et al., 2013; Kendon et al., 2014; Prein et al., 2015), even the most recent climate model data released by the Swiss National Centre for Climate Services has a daily resolution (CH2018, 2018). We performed a post-processing of simulated discharge to estimate sub-daily peak flows by using a constant scaling factor. Another path to derive at sub-daily discharge projections is the temporal disaggregation of precipitation data (see e.g. Sikorska et al., 2018). The influence of this methodological choice on estimated loss could be assessed by including several such methods in the uncertainty assessment.

Finally, the use of the surrogate model itself introduces uncertainty. The surrogate model replaces a fully integrated hydrodynamic simulation of projected peak discharge by using synthetically derived hydrographs for a respective peak magnitude. These hydrographs are an approximation to the real shape of (projected or observed) event hydrographs, and no variation in volumes for a given peak magnitude is considered. Furthermore, the surrogate model is setup for discrete values of flood peak magnitudes and thus interpolation is needed to derive loss estimates on a continuous scale. Zischg et al. (2018b) assessed the uncertainty introduced by these simplifications for a set of nested catchments close to our study area, and with catchment areas between 116 and 2900 km^2. Their validation was based on the number of exposed buildings in the floodplains of the respective catchments for a set of observed flood events. With regard to the error due to interpolation, Zischg et al. (2018b) concluded that the error is small if the interval of modelled peak magnitudes is narrow (they regarded intervals of 50 m^3/s and 100 m^3/s where the first corresponds to the interval used in the present study). In addition, they compared the results obtained by the surrogate model with results stemming from a fully integrated hydrodynamic simulation, as well as with observed data on the number of exposed buildings. They found deviations in the range of 6 to 60% for the overall catchment indicating a large variability of model performance between the different events.

The overall uncertainty associated with the loss estimate of our study amounts to 670 Mio. CHF for the 100-year event. While the smallest estimate indicates a decrease of loss compared to estimations for present day climate, the highest estimates correspond to a more than a 7-fold increase. However, the true uncertainty of future loss is

likely to be greater as we consider selected factors of uncertainty only. Given the wide range of possible outcomes, it remains unclear to which degree flood risk assessments for changed climate conditions can guide practical adaptation decisions at present. In light of the large uncertainties associated with climate change impact assessments, Wilby and Dessai (2010) suggest the development of low-regret adaption strategies that provide benefits irrespective of how the future climate may evolve. This approach seems appropriate even more if we widen the perspective from climate change impact assessments and vulnerability modelling covered in this study to socio-economic projections that can have a large effect on estimated flood damages as well (Alfieri et al., 2015).

5. CONCLUSIONS

Various sources of uncertainty exist along the model chains used for flood loss assessments. Information on such uncertainties is essential for the sensible use of loss estimates and to identify priority areas for further research that aims to reduce existing uncertainties. In the present study, we quantify the importance of four sources of methodological uncertainty affecting the estimation flood loss for changed climate conditions. Using the floodplains of a meso-scale, pre-alpine catchment as a case study area, we investigate the role of scenario-neutral method choice, climate projection uncertainty, hydrological model parametrisation, as well as uncertainty due to choice of a vulnerability function in shaping overall uncertainty. To efficiently simulate a large number of loss estimates, a surrogate inundation model was used. 46500 loss estimates were used for the attribution of uncertainty. The results reveal large uncertainty in the loss estimate for the 100-year flood event that is mainly attributed to vulnerability model formulation. These results indicate that for the study catchment, even in a climate change context (where additional major sources of uncertainties arise), much could be gained by improving vulnerability model formulation. Nonetheless, uncertainty in climate and impact modelling cannot be neglected. The presented study also illustrates how a surrogate inundation model can enable a comprehensive assessment of various sources of uncertainty affecting flood loss estimates.

ACKNOWLEDGEMENTS

This work was funded by the Swiss National Science Foundation (Sinergia NF 17-257). We would like to thank the Swiss Federal Office of Meteorology and Climatology, and the Swiss Federal Office for the Environment for data provision. We thank one reviewer for valuable comments and suggestions.

6. REFERENCES

Alfieri, L., Feyen, L., Dottori, F., & Bianchi, A. (2015). Ensemble flood risk assessment in Europe under high end climate scenarios. *Global Environmental Change*, *35*, 199–212. https://doi.org/10.1016/j.gloenvcha.2015.09.004

Apel, H., Aronica, G. T., Kreibich, H., & Thieken, A. H. (2009). Flood risk analyses—how detailed do we need to be? *Natural Hazards*, *49*(1), 79–98. https://doi.org/10.1007/s11069-008-9277-8

Apel, H., Thieken, A. H., Merz, B., & Blöschl, G. (2004). Flood risk assessment and associated uncertainty. *Natural Hazards and Earth System Science*, *4*(2), 295–308. https://doi.org/10.5194/nhess-4-295-2004

Arnell, N. W., & Gosling, S. N. (2016). The impacts of climate change on river flood risk at the global scale. *Climatic Change*, *134*(3), 387–401. https://doi.org/10.1007/s10584-014-1084-5

Bastola, S., Murphy, C., & Sweeney, J. (2011). The sensitivity of fluvial flood risk in Irish catchments to the range of IPCC AR4 climate change scenarios. *The Science of the Total Environment*, *409*(24), 5403–5415. https://doi.org/10.1016/j.scitotenv.2011.08.042

Bermúdez, M.; Zischg, A.P. (2018). Sensitivity of flood loss estimates to building representation and flow depth attribution methods in micro-scale flood modelling. *Natural Hazards*, 92(3), 1633–48.

Bosshard, T., Carambia, M., Goergen, K., Kotlarski, S., Krahe, P., Zappa, M., & Schär, C. (2013). Quantifying uncertainty sources in an ensemble of hydrological climate-impact projections. *Water Resources Research*, *49*(3), 1523–1536. https://doi.org/10.1029/2011WR011533

Bubeck, P., Moel, H. de, Bouwer, L. M., & Aerts, J. C. J. H. (2011). How reliable are projections of future flood damage? *Natural Hazards and Earth System Sciences*, *11*(12), 3293–3306. https://doi.org/10.5194/nhess-11-3293-2011

CH2018. (2018). *CH2018 - Climate Scenarios for Switzerland: Technical Report*. Zurich: National Centre for Climate Services.

Chen, J., Brissette, F. P., Poulin, A., & Leconte, R. (2011). Overall uncertainty study of the hydrological impacts of climate change for a Canadian watershed. *Water Resources Research*, *47*(12), 176. https://doi.org/10.1029/2011WR010602

Dams, J., Nossent, J., Senbeta, T. B., Willems, P., & Batelaan, O. (2015). Multi-model approach to assess the impact of climate change on runoff. *Journal of Hydrology*, *529*, 1601–1616. https://doi.org/10.1016/j.jhydrol.2015.08.023

Dutta, D., Herath, S., & Musiake, K. (2003). A mathematical model for flood loss estimation. *Journal of Hydrology*, *277*(1-2), 24–49. https://doi.org/10.1016/S0022-1694(03)00084-2

Falter, D., Schröter, K., Dung, N. V., Vorogushyn, S., Kreibich, H., Hundecha, Y., . . . Merz, B. (2015). Spatially coherent flood risk assessment based on long-term continuous simulation with a coupled model chain. *Journal of Hydrology*, *524*, 182–193. https://doi.org/10.1016/j.jhydrol.2015.02.021

Felder, G., Gómez-Navarro, J. J., Zischg, A. P., Raible, C. C., Röthlisberger, V., Bozhinova, D., . . . Weingartner, R. (2018). From global circulation to local flood loss: Coupling models across the scales. *The Science of the Total Environment*, *635*, 1225–1239. https://doi.org/10.1016/j.scitotenv.2018.04.170

Felder, G., Zischg, A., & Weingartner, R. (2017). The effect of coupling hydrologic and hydrodynamic models on probable maximum flood estimation. *Journal of Hydrology*, *550*, 157–165. https://doi.org/10.1016/j.jhydrol.2017.04.052

Frei, C. (2014). Interpolation of temperature in a mountainous region using nonlinear profiles and non-Euclidean distances. *International Journal of Climatology*, *34*(5), 1585–1605. https://doi.org/10.1002/joc.3786

Frei, C., Schöll, R., Fukutome, S., Schmidli, J., & Vidale, P. L. (2006). Future change of precipitation extremes in Europe: Intercomparison of scenarios from regional climate models. *Journal of Geophysical Research*, *111*(D6). https://doi.org/10.1029/2005JD005965

Gerl, T., Kreibich, H., Franco, G., Marechal, D., & Schröter, K. (2016). A Review of Flood Loss Models as Basis for Harmonization and Benchmarking. *PloS One*, *11*(7), e0159791. https://doi.org/10.1371/journal.pone.0159791

Gregersen, I. B., Sørup, H. J. D., Madsen, H., Rosbjerg, D., Mikkelsen, P. S., & Arnbjerg-Nielsen, K. (2013). Assessing future climatic changes of rainfall extremes at small spatio-temporal scales. *Climatic Change*, *118*(3-4), 783–797. https://doi.org/10.1007/s10584-012-0669-0

Hattermann, F. F., Huang, S., Burghoff, O., Willems, W., Österle, H., Büchner, M., & Kundzewicz, Z. (2014). Modelling flood damages under climate change conditions – a case study for Germany. *Natural Hazards and Earth System Sciences*, *14*(12), 3151–3168. https://doi.org/10.5194/nhess-14-3151-2014

Hydrotec. (2011). *Hochwasser-Aktionsplan Angerbach. Teil I: Berichte und Anlagen: Studie im Auftrag des Stua Dusseldorf*. Aachen.

Jacob, D., Petersen, J., Eggert, B., Alias, A., Christensen, O. B., Bouwer, L. M., . . . Yiou, P. (2014). EURO-CORDEX: New high-resolution climate change projections for European impact research. *Regional Environmental Change*, *14*(2), 563–578. https://doi.org/10.1007/s10113-013-0499-2

Jonkman, S. N., Bočkarjova, M., Kok, M., & Bernardini, P. (2008). Integrated hydrodynamic and economic modelling of flood damage in the Netherlands. *Ecological Economics*, *66*(1), 77–90. https://doi.org/10.1016/j.ecolecon.2007.12.022

Jung, I.-W., Chang, H., & Moradkhani, H. (2011). Quantifying uncertainty in urban flooding analysis considering hydro-climatic projection and urban development effects. *Hydrology and Earth System Sciences*, *15*(2), 617–633. https://doi.org/10.5194/hess-15-617-2011

Karlsson, I. B., Sonnenborg, T. O., Refsgaard, J. C., Trolle, D., Børgesen, C. D., Olesen, J. E., . . . Jensen, K. H. (2016). Combined effects of climate models, hydrological model structures and land use scenarios on hydrological impacts of climate change. *Journal of Hydrology*, *535*, 301–317. https://doi.org/10.1016/j.jhydrol.2016.01.069

Kay, A. L., Davies, H. N., Bell, V. A., & Jones, R. G. (2009). Comparison of uncertainty sources for climate change impacts: Flood frequency in England. *Climatic Change*, *92*(1-2), 41–63. https://doi.org/10.1007/s10584-008-9471-4

Keller, L., Rössler, O., Martius, O., & Weingartner, R. (2018). Comparison of scenario-neutral approaches for estimation of climate change impacts on flood characteristics. Hydrological Processes, 33(4), 535–550. https://doi.org/10.1002/hyp.13341

Kendon, E. J., Roberts, N. M., Fowler, H. J., Roberts, M. J., Chan, S. C., & Senior, C. A. (2014). Heavier summer downpours with climate change revealed by weather forecast resolution model. *Nature Clim. Change*, *4*(7), 570–576. https://doi.org/10.1038/nclimate2258

Martins, E. S., & Stedinger, J. R. (2000). Generalized maximum-likelihood generalized extreme-value quantile estimators for hydrologic data. *Water Resources Research*.

Merz, B., & Thieken, A. H. (2009). Flood risk curves and uncertainty bounds. *Natural Hazards*, *51*(3), 437–458. https://doi.org/10.1007/s11069-009-9452-6

Moel, H. de, & Aerts, J. C. J. H. (2011). Effect of uncertainty in land use, damage models and inundation depth on flood damage estimates. *Natural Hazards*, *58*(1), 407–425. https://doi.org/10.1007/s11069-010-9675-6

Moel, H. de, Asselman, N. E. M., & Aerts, J. C. J. H. (2012). Uncertainty and sensitivity analysis of coastal flood damage estimates in the west of the Netherlands. Natural Hazards and Earth System Sciences, 12(4), 1045–1058. https://doi.org/10.5194/nhess-12-1045-2012

Moel, H. de, Bouwer, L. M., & Aerts, J. C. J. H. (2014). Uncertainty and sensitivity of flood risk calculations for a dike ring in the south of the Netherlands. *The Science of the Total Environment*, *473-474*, 224–234. https://doi.org/10.1016/j.scitotenv.2013.12.015

Papathoma-Köhle, M., Zischg, A., Fuchs, S., Glade, T., & Keiler, M. (2015). Loss estimation for landslides in mountain areas – An integrated toolbox for vulnerability assessment and damage documentation. *Environmental Modelling & Software*, *63*, 156–169. https://doi.org/10.1016/j.envsoft.2014.10.003

Paquet, E., Garavaglia, F., Garçon, R., & Gailhard, J. (2013). The SCHADEX method: A semi-continuous rainfall–runoff simulation for extreme flood estimation. Journal of Hydrology, 495, 23–37. https://doi.org/10.1016/j.jhydrol.2013.04.045

Prein, A. F., Langhans, W., Fosser, G., Ferrone, A., Ban, N., Goergen, K., . . . Leung, R. (2015). A review on regional convection-permitting climate modelling: Demonstrations, prospects, and challenges. *Reviews of Geophysics (Washington, D.C. : 1985)*, *53*(2), 323–361. https://doi.org/10.1002/2014RG000475

Prudhomme, C., Wilby, R. L., Crooks, S., Kay, A. L., & Reynard, N. S. (2010). Scenario-neutral approach to climate change impact studies: Application to flood risk. *Journal of Hydrology*, *390*(3-4), 198–209. https://doi.org/10.1016/j.jhydrol.2010.06.043

Pushpalatha, R., Perrin, C., Le Moine, N., Mathevet, T., & Andréassian, V. (2011). A downward structural sensitivity analysis of hydrological models to improve low-flow simulation. *Journal of Hydrology*, *411*(1-2), 66–76. https://doi.org/10.1016/j.jhydrol.2011.09.034

Ratto, M., Castelletti, A., & Pagano, A. (2012). Emulation techniques for the reduction and sensitivity analysis of complex environmental models. *Environmental Modelling & Software*, *34*, 1–4. https://doi.org/10.1016/j.envsoft.2011.11.003

Razavi, S., Tolson, B. A., & Burn, D. H. (2012a). Numerical assessment of metamodelling strategies in computationally intensive optimization. *Environmental Modelling & Software*, *34*, 67–86. https://doi.org/10.1016/j.envsoft.2011.09.010

Razavi, S., Tolson, B. A., & Burn, D. H. (2012b). Review of surrogate modelling in water resources. *Water Resources Research*, *48*(7), 559. https://doi.org/10.1029/2011WR011527

Röthlisberger, V., Zischg, A. P., & Keiler, M. (2017). Identifying spatial clusters of flood exposure to support decision making in risk management. *The Science of the Total Environment*, *598*, 593–603. https://doi.org/10.1016/j.scitotenv.2017.03.216

Röthlisberger, V., Zischg, A. P., & Keiler, M. (2018). A comparison of building value models for flood risk analysis. *Natural Hazards and Earth System Sciences*, *18*, 2431-2453.

Semenov, M. A., & Barrow, E. M. (1997). Use of a stochastic weather generator on the development of climate change scenarios. *Climatic Change*.

Semenov, M. A., Brooks, R. J., Barrow, E. M., & Richardson, C. W. (1998). Comparison of the WGEN and LARS-WG stochastic weather generators for diverse climates. *Climate Research*, *10*, 95–107. https://doi.org/10.3354/cr010095

Sikorska, A. E., Viviroli, D., & Seibert, J. (2018). Effective precipitation duration for runoff peaks based on catchment modelling. *Journal of Hydrology*, *556*, 510–522. https://doi.org/10.1016/j.jhydrol.2017.11.028

Steiner, S. (2007). *Emme-Hochwasser: Dokumentation, Typisierung und Analyse der 25 grössten Ereignisse von 1930-2005*. *Publikation Gewässerkunde: Vol. 377*. Bern.

Steinschneider, S., Wi, S., & Brown, C. M. (2015). The integrated effects of climate and hydrologic uncertainty on future flood risk assessments. *Hydrological Processes*, *29*(12), 2823–2839. https://doi.org/10.1002/hyp.10409

Tiefbauamt des Kantons Bern Oberingenieurkreis IV (TBA-OIK IV) (Ed.). (2005). Befreite Emme, lebendiger Fluss: Naturnaher Wasserbau bringt den Geschiebehaushalt der Emme wieder ins Gleichgewicht [Special issue]. Burgdorf.

Totschnig, R., Sedlacek, W., & Fuchs, S. (2011). A quantitative vulnerability function for fluvial sediment transport. *Natural Hazards*, *58*(2), 681–703. https://doi.org/10.1007/s11069-010-9623-5

Valéry, A., Andréassian, V., & Perrin, C. (2014). 'As simple as possible but not simpler': What is useful in a temperature-based snow-accounting routine? Part 2 – Sensitivity analysis of the Cemaneige snow accounting routine on 380 catchments. *Journal of Hydrology*, *517*, 1176–1187. https://doi.org/10.1016/j.jhydrol.2014.04.058

Vormoor, K., Rössler, O., Bürger, G., Bronstert, A., & Weingartner, R. (2017). When timing matters-considering changing temporal structures in runoff response surfaces. *Climatic Change*, *409*(24), 5403. https://doi.org/10.1007/s10584-017-1940-1

Wilby, R. L., & Dessai, S. (2010). Robust adaptation to climate change. *Weather*, *65*(7), 180–185. https://doi.org/10.1002/wea.543

Wing, O. E. J., Bates, P. D., Smith, A. M., Sampson, C. C., Johnson, K. A., Fargione, J., & Morefield, P. (2018). Estimates of present and future flood risk in the conterminous United States. Environmental Research Letters, 13(3), 034023. https://doi.org/10.1088/1748-9326/aaac65

Zischg, A.P., Felder, G., Weingartner, R., Quinn, N., Coxon, G., Neal, J., Freer, J., Bates, P., (2018a). Effects of variability in probable maximum precipitation patterns on flood losses. *Hydrology and Earth System Sciences*. 22 (5), 2759–2773.

Zischg, A. P., Felder, G., Mosimann, M., Röthlisberger, V., & Weingartner, R. (2018b). Extending coupled hydrological-hydraulic model chains with a surrogate model for the estimation of flood losses. *Environmental Modelling & Software*, *108*, 174–185. https://doi.org/10.1016/j.envsoft.2018.08.009

Zischg, A. P., Hofer, P., Mosimann, M., Röthlisberger, V., Ramirez, J. A., Keiler, M., & Weingartner, R. (2018c). Flood risk (d)evolution: Disentangling key drivers of flood risk change with a retro-model experiment. *The Science of the Total Environment*, *639*, 195–207. https://doi.org/10.1016/j.scitotenv.2018.05.056

Graphical abstract

Highlights

- Quantification of epistemic uncertainties affecting estimates of flood loss for changed climate conditions
- Use of surrogate inundation model for large ensemble flood loss modelling for a meso-scale, pre-alpine catchment
- Vulnerability function choice explains almost half of variance in loss estimate
- Uncertainty in flood peak estimate for changed climate conditions nearly as important

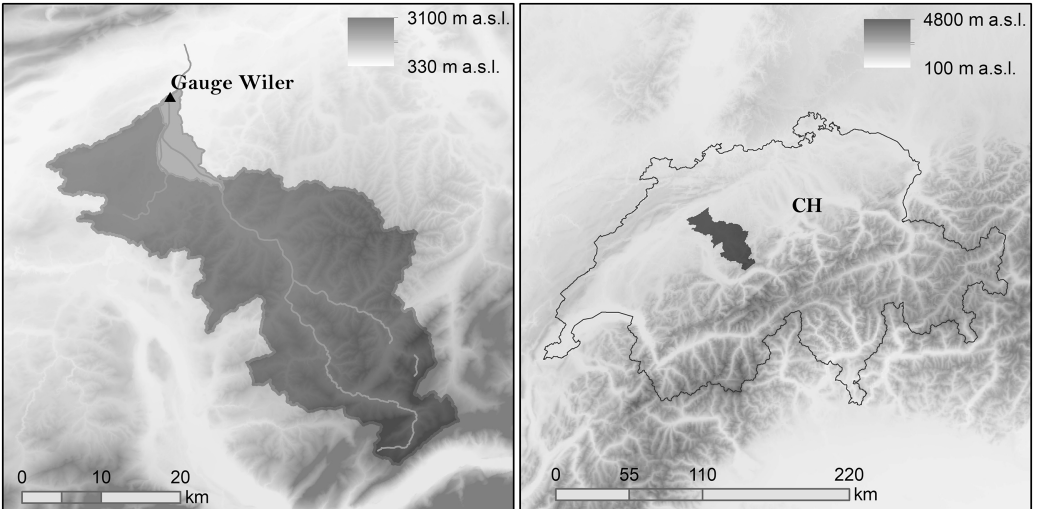
3100 m a.s.l.
330 m a.s.l.
Gauge Wiler
0
10
20
km
4800 m a.s.l.
100 m a.s.l.
CH
0
55
110
220
km

Figure 1

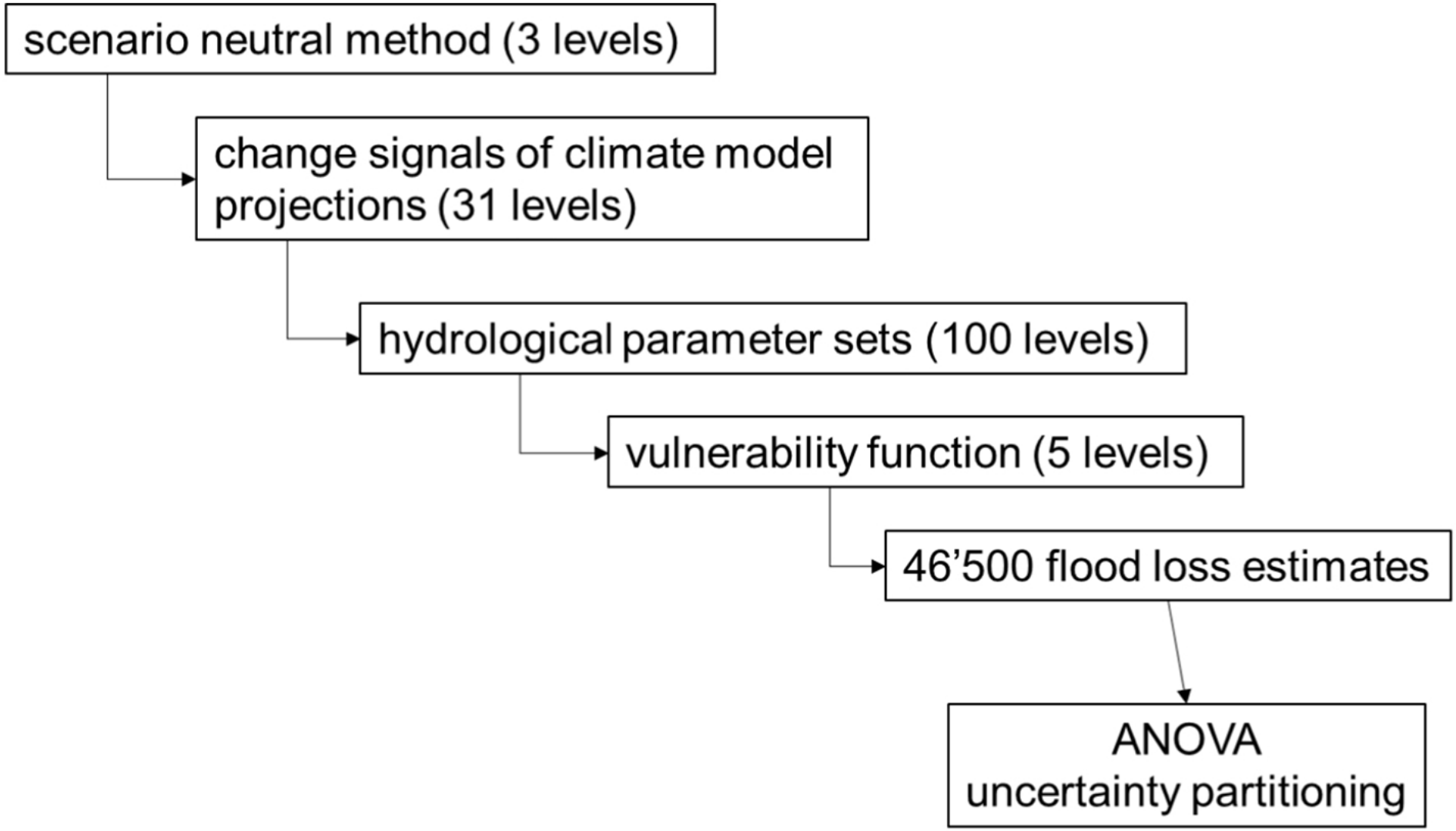
scenario neutral method (3 levels)
change signals of climate model projections (31 levels)
hydrological parameter sets (100 levels)
vulnerability function (5 levels)
46’500 flood loss estimates
ANOVA
uncertainty partitioning

Figure 2

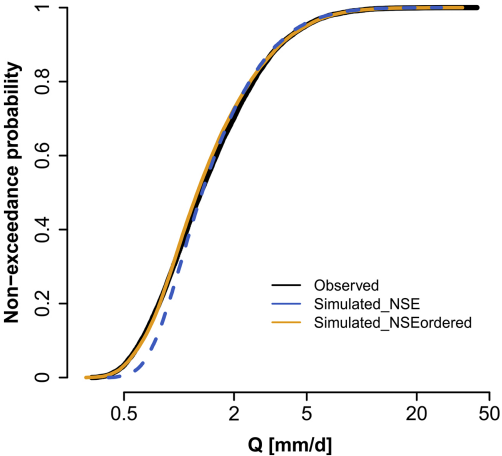
Non−exceedance probability
0
0.2
0.4
0.6
0.8
1
0.5
2
5
20
50
Q [mm/d]
Observed
Simulated_NSE
Simulated_NSEordered

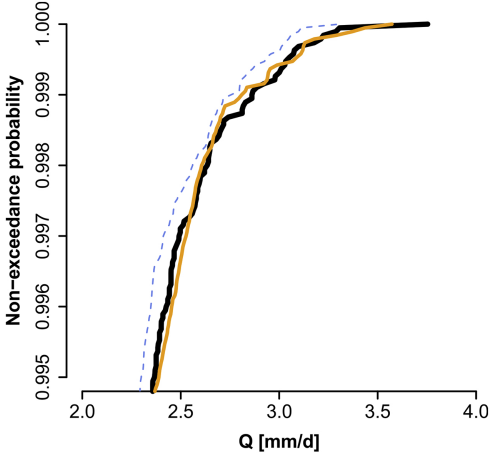
Non−exceedance probability
0.995
0.996
0.997
0.998
0.999
1.000
2.0
2.5
3.0
3.5
4.0
Q [mm/d]

Figure 3

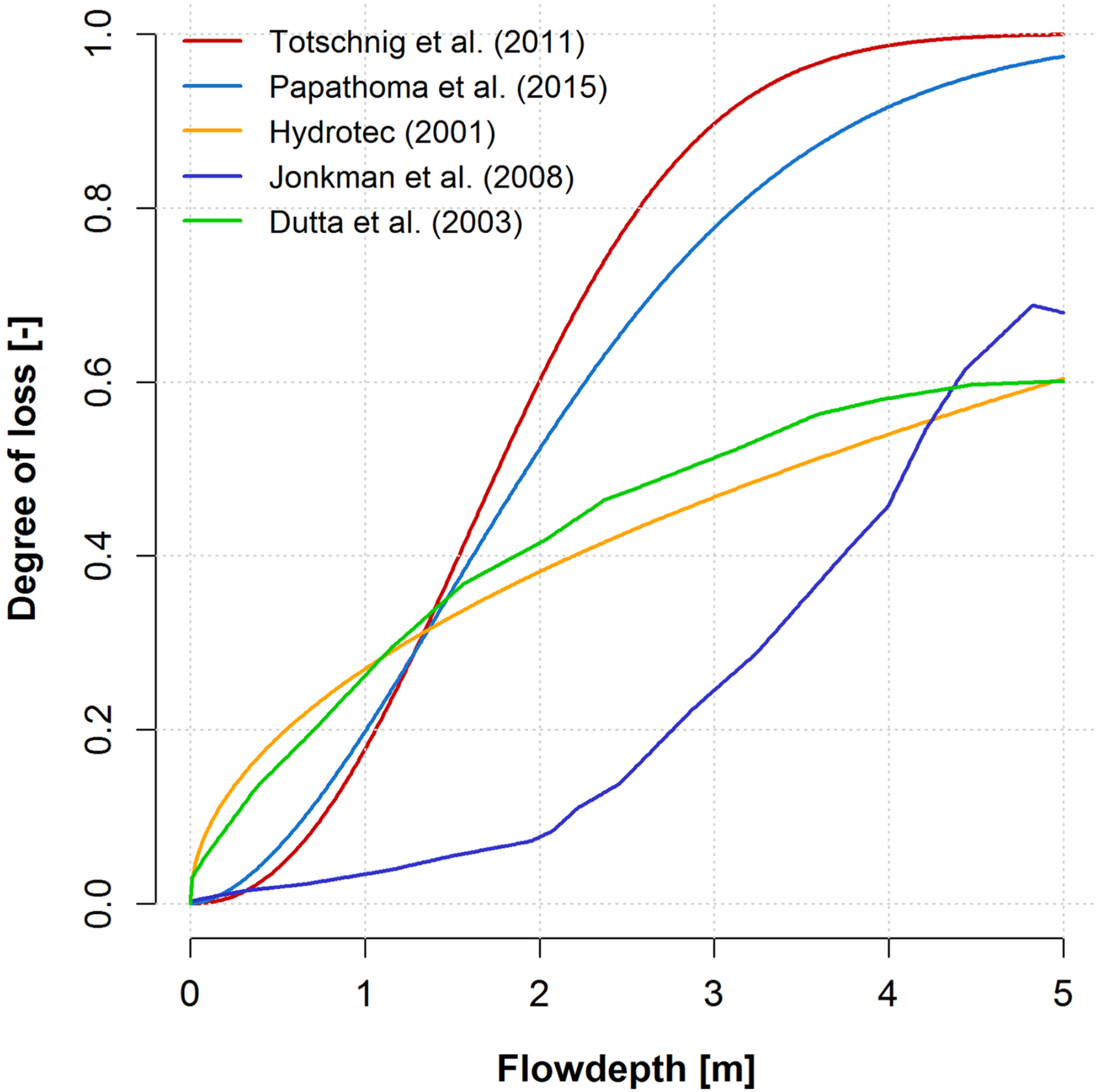
Totschnig et al. (2011)
Papathoma et al. (2015)
Hydrotec (2001)
Jonkman et al. (2008)
Dutta et al. (2003)
Degree of loss [-]
0.0
0.2
0.4
0.6
0.8
1.0
0
1
2
3
4
5
Flowdepth [m]

Figure 4

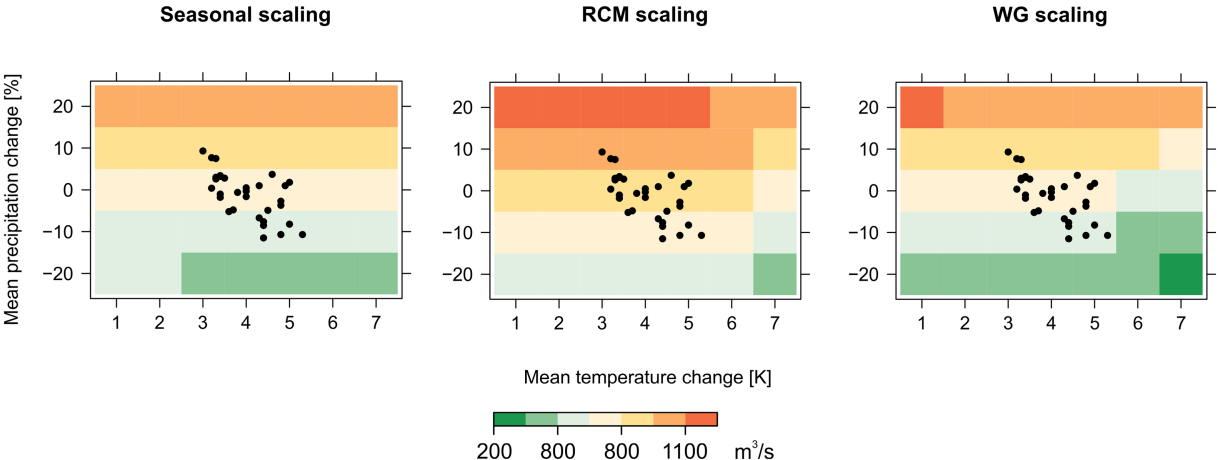
Seasonal scaling
RCM scaling
WG scaling
Mean precipitation change [%]
20
10
0
−10
−20
1
2
3
4
5
6
7
Mean temperature change [K]
200
800
800
1100
m3/s

Figure 5

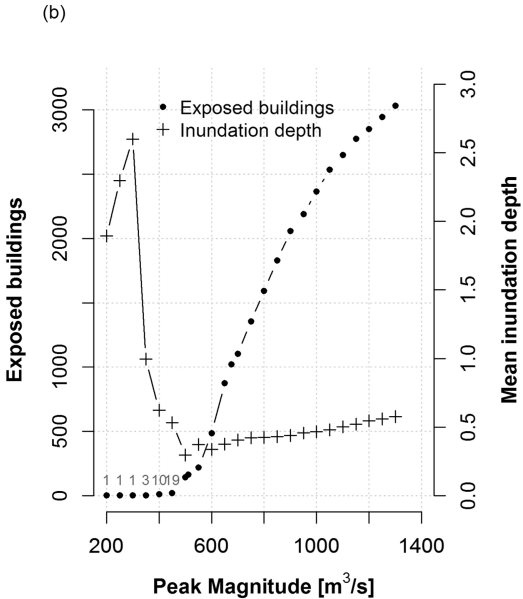
(b)
Exposed buildings
Inundation depth
Exposed buildings
Mean inundation depth
Peak Magnitude [m3/s]
1 1 1 3 10 19
0
500
1000
2000
3000
0.0
0.5
1.0
1.5
2.0
2.5
3.0
200
600
1000
1400

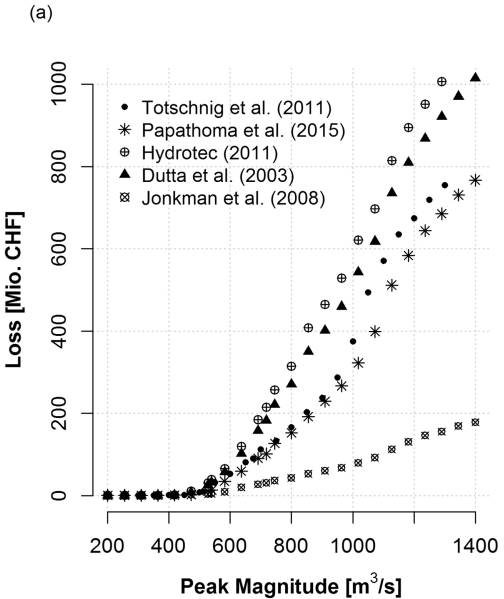
(a)
Totschnig et al. (2011)
Papathoma et al. (2015)
Hydrotec (2011)
Dutta et al. (2003)
Jonkman et al. (2008)
Loss [Mio. CHF]
Peak Magnitude [m3/s]
0
200
400
600
800
1000
200
400
600
800
1000
1400

Figure 6

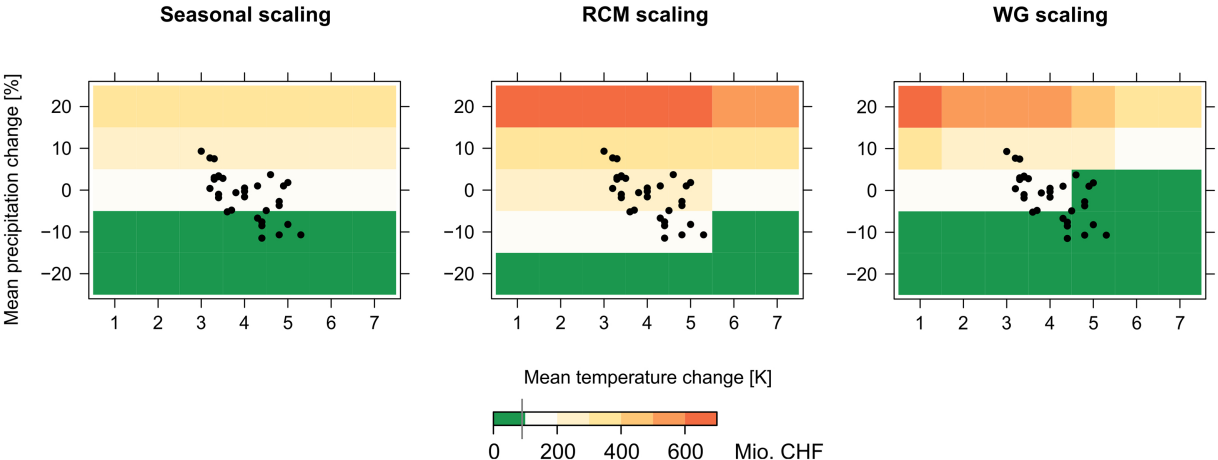
Seasonal scaling
RCM scaling
WG scaling
Mean precipitation change [%]
20
10
0
−10
−20
1
2
3
4
5
6
7
Mean temperature change [K]
0
200
400
600
Mio. CHF

Figure 7

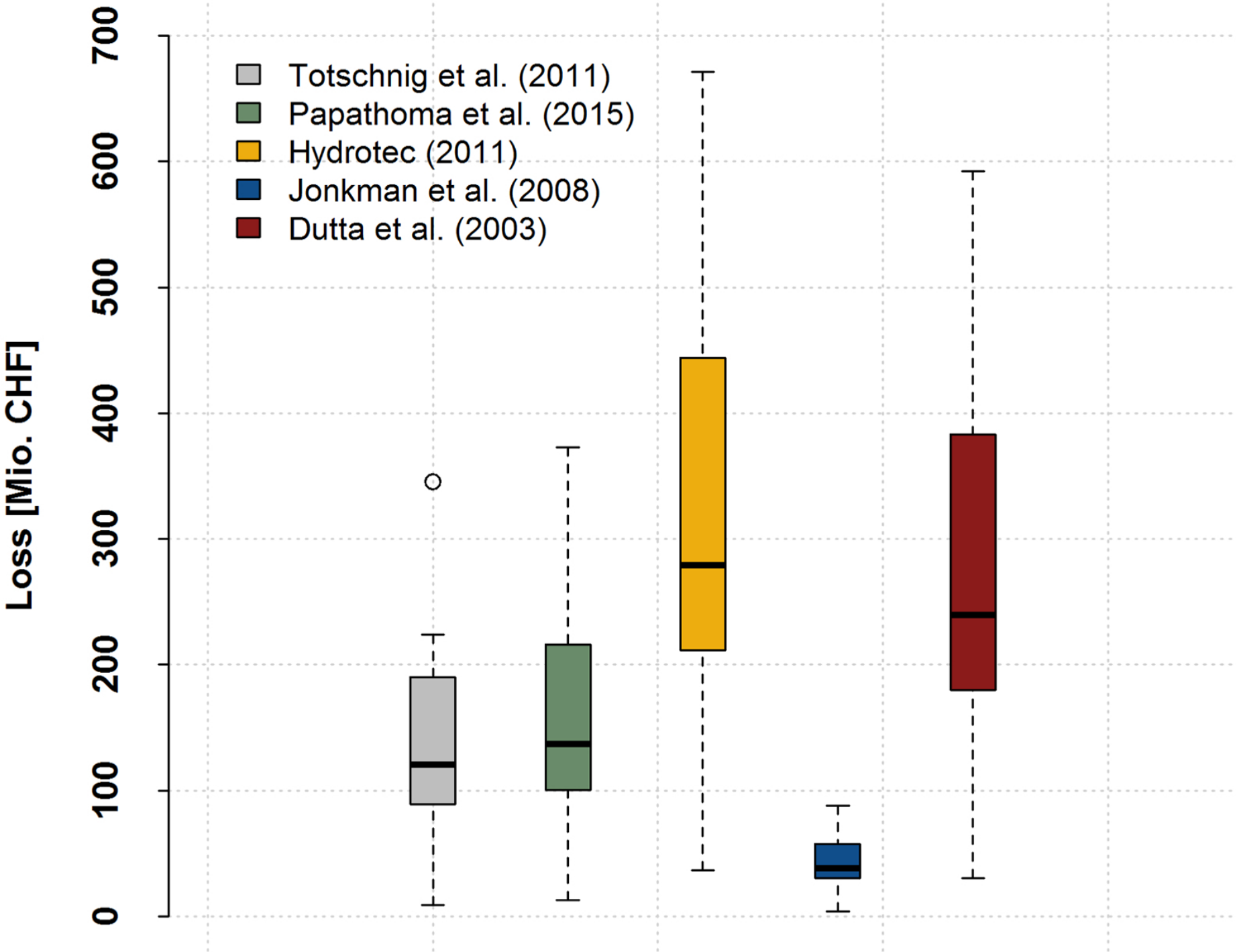
Totschnig et al. (2011)
Papathoma et al. (2015)
Hydrotec (2011)
Jonkman et al. (2008)
Dutta et al. (2003)
Loss [Mio. CHF]
0
100
200
300
400
500
600
700

Figure 8